analytical chemistry

pubs.acs.org/ac Article

Novel Luminescent Nanostructured Coordination Polymer: Facile Fabrication and Application in Electrochemiluminescence Biosensor for microRNA-141 Detection

Cun Wang, Qian Han, Fangjing Mo, Min Chen, Zhengwei Xiong, and Yingzi Fu*

Cite This: *Anal. Chem.* 2020, 92, 12145−12151 Read Online

ACCESS | Metrics & More | Article Recommendations | Supporting Information

ABSTRACT: A series of novel luminescent nanostructured coordination polymers (Ce−Ru−NCPs) with tunable morphologies have been successfully synthesized on a large scale at room temperature by a facile and rapid solution-phase method using Ce^{3+} and tris(4,4′-dicarboxylicacid-2,2′-bipyridyl) ruthenium(II) dichloride ($Ru(dcbpy)_3^{2+}$). Among them, the flowerlike Ce−Ru−NCP shows good cathodic electrochemiluminescence (ECL) characteristics. The ECL efficiency of the Ce−Ru−NCP/$S_2O_8^{2-}$ system is about 2.34 times that of the classic tris(2,2′-bipyridyl) ruthenium(II) dichloride/$S_2O_8^{2-}$ ($Ru(bpy)_3^{2+}$/$S_2O_8^{2-}$) system. Hence, we report a sensitive ECL biosensor for microRNA-141 (miRNA-141) detection based on the flowerlike Ce−Ru−NCP as a cathodic ECL luminophore and a bipedal three-dimensional (3D) DNA walking machine as a signal amplifier. Through the bipedal 3D DNA walking machine, trace targets can be converted to substantial secondary targets (marked with the quencher dopamine), and a significant quenching effect on the ECL signal is achieved. As a result, the proposed biosensor exhibits a relatively good sensitivity for miRNA-141 detection and shows a dynamic range from 1.0×10^{-16} to 1.0×10^{-6} mol·L^{-1} with a limit of detection (LOD) of 33 amol·L^{-1} ($S/N = 3$). The Ce−Ru−NCP with tunable morphologies and high ECL efficiency, intensity, and stability possesses potential applications in ECL analysis.

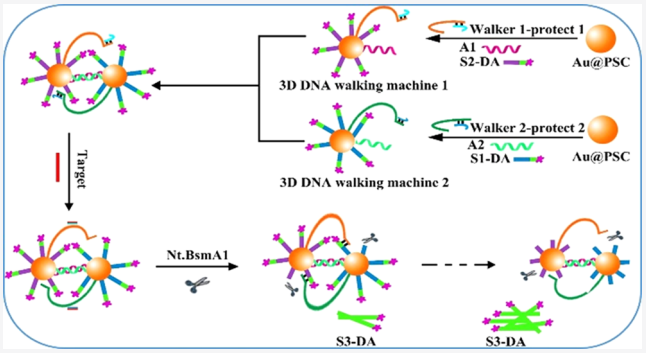

INTRODUCTION

Electrochemiluminescence (ECL) combining the advantages of electrochemistry and chemiluminescence is an important detection method with low background signal and high sensitivity.[1,2] The ECL luminophore plays a key role in the transformation from electrical energy into radiative energy.[2,3] Cathodic luminophores such as quantum dots, metal nanoclusters, tetraphenylethene derivatives, tris(2,2′-bipyridyl) ruthenium(II) ($Ru(bpy)_3^{2+}$), and so on have been applied to construct the ECL biosensors.[3−5] However, these conventional cathodic luminophores exhibit weak ECL emission and require a more negative ECL potential than −1.0 V, some even at −2.0 V.[2,4] However, higher potential causes the emission of oxygen in the electrolyte and damage to the biomolecules and electrode,[3,6] causes a larger background signal for the biosensor, and limits the practical application. Therefore, the synthesis of a novel cathodic ECL luminophore with a relatively lower potential is of great significance.

$Ru(bpy)_3^{2+}$ and its derivatives, such as tris(4,4′-dicarboxylicacid-2,2′-bipyridyl) ruthenium(II) dichloride ($Ru(dcbpy)_3^{2+}$), are the most important and classic ECL luminophores. They possess the advantages of high ECL activity, long excited state, and superior electrochemical reversibility and have been applied in many fields including the ECL biosensors.[1,5] To further improve the ECL efficiency, some nanomaterials have been synthesized,[5,7,8] such as metal−organic frameworks (MOFs), metal−organic layers (MOLs), etc., and used as supporting matrices to immobilize $Ru(bpy)_3^{2+}$ or $Ru(dcbpy)_3^{2+}$. Although the ECL efficiency has been improved to some extent, the preparation and application of these nanomaterials still face challenges. First, the ECL signal may be quenched by some carrier materials.[9,10] Second, the relatively low specific surface area of MOLs, or the mismatched size between the MOFs and the luminophores, which suppresses the massive adsorption of the luminophores or causes the leak of the luminophores during the detection process, leads to poor stability and low ECL intensity.[8] Third, the insulating ligands of the MOFs and MOLs may restrain the electronic excitation of the luminophores, resulting in a relatively low ECL efficiency.[11] Thus, our group has successfully synthesized a novel luminescence-functionalized

Received: January 10, 2020
Accepted: August 11, 2020
Published: August 11, 2020

https://dx.doi.org/10.1021/acs.analchem.0c00130
Anal. Chem. 2020, 92, 12145−12151

Table 1. Summary of the Experimental Conditions and the Corresponding Morphologies of the Ce−Ru−NCPs

sample	c_{Ce}/c_{Ru}[a]	PVP (g)	ethanol/water	morphology	length (μm)	yield	ECL intensity (au)
A	40:1		pure water	flower	0.9	high	17 368
B	40:1		pure ethanol	honeycomb	2.0	low	15 053
C	40:1	1.0	pure water	hill	1.0	high	14 044
D	40:1	1.0	pure ethanol	hump	1.5	low	13 362
E	40:1		1:1	flake	0.1	high	16 950
F	10:1		1:1	net	0.3	high	13 880
G	5:1		1:1	snow	0.5	high	9809

[a]Molar concentration ratio.

Ru−metal−organic framework (MOF) nanoflower with Ru(dcbpy)$_3^{2+}$ as the organic ligand,[12] which endows the ECL sensor with good sensitivity and high stability. However, the synthesis method of Ru−MOF nanoflower is complicated, time-consuming, and low-yielding, making it difficult to meet the requirements of large-scale production. Therefore, it is still imperative and challenging to seek a new method for facile, rapid, large-scale, high-yielding, and economical synthesis of the novel ECL luminophore directly using Ru(bpy)$_3^{2+}$ or Ru(dcbpy)$_3^{2+}$ as organic ligands.

Nanostructured coordination polymer (NCP) with lanthanide ion (Ln^{3+}) as the coordination center atom has aroused great interest among scientists since the high coordination requirement/number (vs transition metals), unique optical, and electronic and photoluminescent properties derived from f-to-f electron transitions in the $4f^n$ shell.[13,14] For example, Ce^{3+} is capable of absorbing and emitting light with a high quantum yield, which can significantly improve the luminous intensity of Ce^{3+}-based NCP.[15,16] Ru(dcbpy)$_3^{2+}$, a derivative of Ru(bpy)$_3^{2+}$, contains six carboxyl groups with strong coordination ability and multiple coordination modes and exhibits good luminescence properties, allowing it to be used as a ligand in NCP.[17] The above concepts provide a certain basis for the synthesis of new luminescent NCP.

Diverse amplification techniques, such as polymerase chain reaction (PCR), catalyzed hairpin assembly (CHA), and strand displacement amplification (SDA), have been employed in further improving the sensitivity of ECL biosensors.[18−21] However, they generally suffer from harsh reaction conditions and complicated reaction processes as well as the false-positive or false-negative signals in the experimental results.[22] As one of the most important member of DNA nanomachines, a three-dimensional (3D) DNA walking machine can move progressively and autonomously along the highly ordered tracks to release a large number of secondary targets.[23] For instance, immune recognition induced,[24] single- or dual-enzyme-driven,[25,26] and toehold-mediated strand displacement reaction-controlled 3D DNA walking machines[27] have been constructed. Nevertheless, the reported 3D DNA walking machines in recent years have been limited to walking on a single foot, which brings about inefficiency and relative weakness in target output capabilities. Therefore, it is of great significance to design a bipedal- or multilegged 3D DNA walking machine with high efficiency and high secondary target output capability.

Inspired by the above concepts, a flowerlike luminescence-functionalized NCP (Ce−Ru−NCP) with a strong and stable ECL signal was synthesized using Ce^{3+} as the central coordination atom and Ru(dcbpy)$_3^{2+}$ as the ligand. Ce−Ru−NCP is synthesized in a simple, rapid, and large-scale method at room temperature. Moreover, the ECL efficiency of Ce−Ru−NCP/$S_2O_8^{2-}$ system is higher than that of the classic Ru(bpy)$_3^{2+}$/$S_2O_8^{2-}$ system ($S_2O_8^{2-}$ as a co-reaction reagent). In addition, with the help of the amplification technique of the bipedal 3D DNA walking machine, a novel ECL biosensor has been designed to detect miRNA-141 sensitively, which provides a novel idea for biological analysis and clinical analysis.

EXPERIMENTAL SECTION

Synthesis of Ce−Ru−NCPs, AuNPs, and Au@PSC. The flowerlike Ce−Ru−NCP was synthesized as follows: 1 mL of $Ce(NO_3)_3$ (0.05 mmol) aqueous solution (pH 3.5) was added dropwise into 40 mL of Ru(dcbpy)$_3^{2+}$ (0.05 mmol) solution under vigorous stirring at room temperature and a large amount of orange-red precipitate was generated immediately. After stirring for 10 min, the orange-red precipitate was collected by centrifugation at 5000 rpm for 1 min and washed several times with water. A series of different morphologies of Ce−Ru−NCP were prepared by adjusting the experiment conditions while other reaction parameters remained unchanged (Table 1). Moreover, gold nanoparticles (AuNPs), gold, and amino-modified magnetic polystyrene microsphere nanocomposite (Au@PSC) were prepared according to the literature[21,28] (see the Supporting Information, SI).

Preparation of the Bipedal 3D DNA Walking Machine. The bipedal 3D DNA walking machine was prepared by joining two separate 3D DNA walking machines (1 and 2). The specific process is as follows: first, 250 μL of the carboxylic acid modified support DNA 1 (S1, 6 μmol·L^{-1}) was activated by EDC/NHS (4:1) solution for 2 h at 4 °C. Then, massive dopamine (DA) was added to the solution and stirred at 4 °C for 2 h to obtain the DA marked S1 (S1-DA). Similarly, S2-DA was obtained. Second, the walker probe 1−protect DNA 1 (walker 1−protect 1) was prepared by mixing 2 μL of 2 μmol·L^{-1} protect 1 and 2 μL of 2 μmol·L^{-1} walker 1 together for 2 h at 37 °C. The walker 2−protect 2 was obtained in the same way. Third, 4 μL of walker 1−protect 1 (1 μmol·L^{-1}), 80 μL of S2-DA (2 μmol·L^{-1}), 2 μL of DNA strand A1 (2 μmol·L^{-1}), and 50 μL of Au@PSC were mixed and shaken overnight to get the 3D DNA walking machine 1 via Au−S bond. The 3D DNA walking machine 2 was gained in the same way by mixing Au@PSC, walker 2−protect 2, S1-DA, and A2. Fourth, the bipedal 3D DNA walking machine was obtained by linking the 3D DNA walking machines 1 and 2 together via A1 and A2. Fifth, after the magnetic separation, the obtained bipedal 3D DNA walking machine was redispersed in 136 μL of 20 mmol·L^{-1} Tris−HCl (pH 7.0) to get rid of the raw DNA left, then 2 μL of different concentrations of miRNA-141 was added and incubated at 37 °C for 2 h to release the walker 1 and walker 2. Due to the Watson−Crick base pairing, the released walker 1 was hybridized with S1-DA and walker 2 was

https://dx.doi.org/10.1021/acs.analchem.0c00130
Anal. Chem. 2020, 92, 12145−12151

Scheme 1. Construction of the ECL Biosensor and Assembly Process of the Bipedal 3D DNA Walking Machine

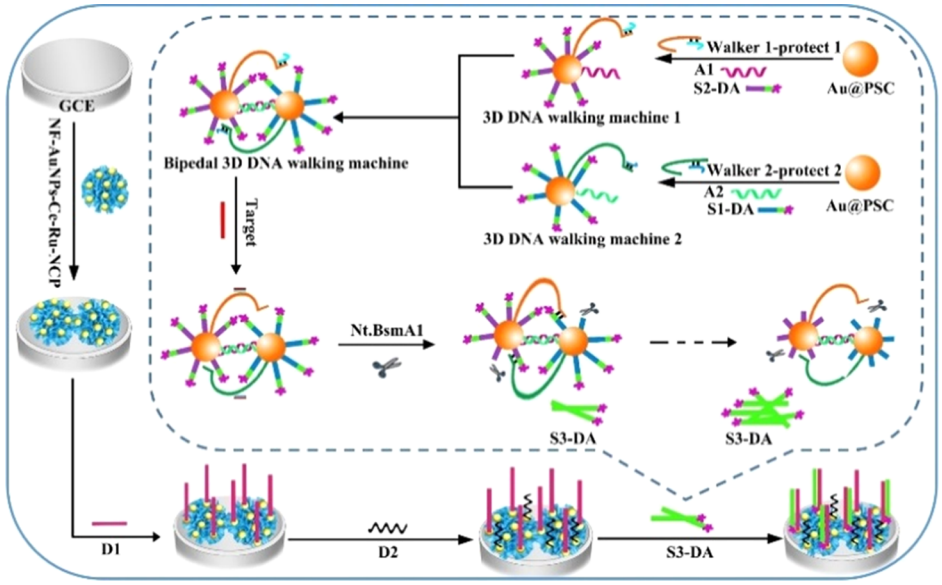

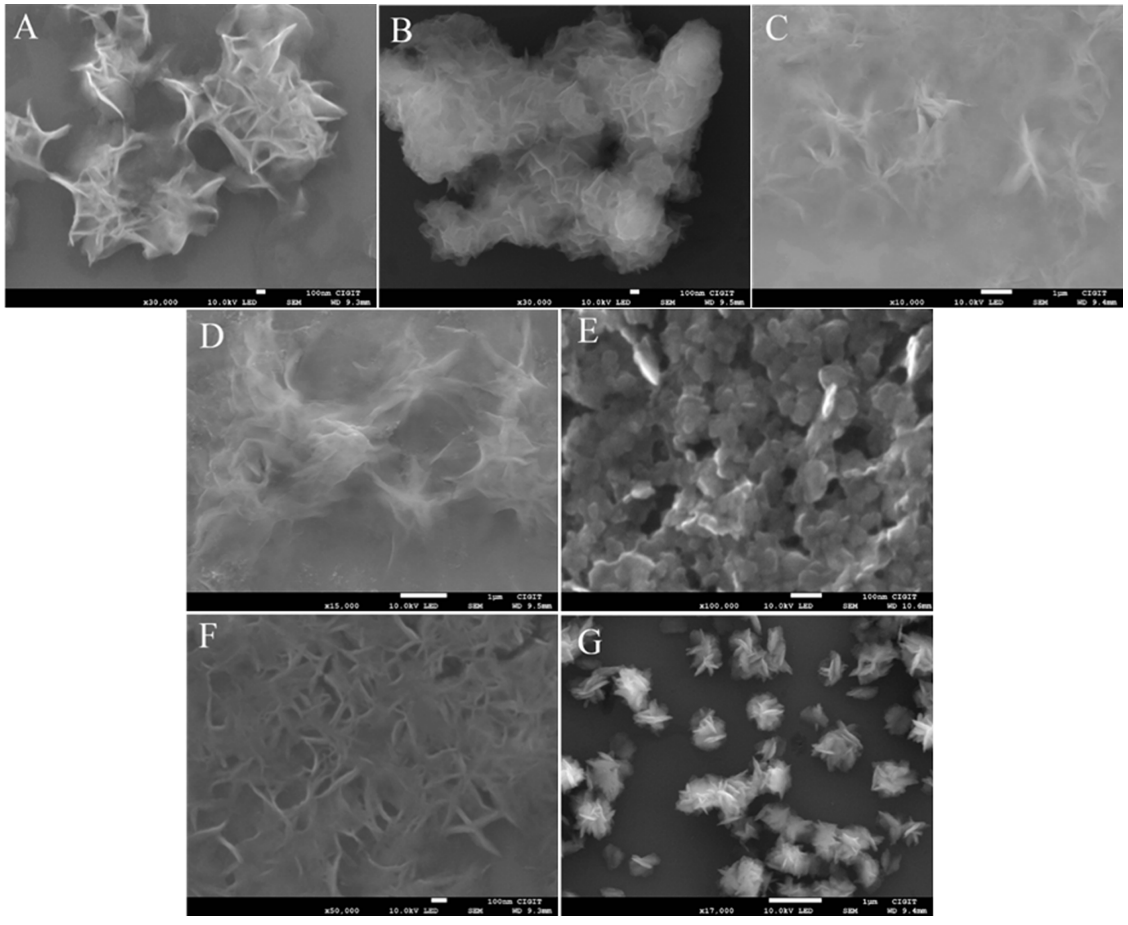

Figure 1. (A–G) SEM images of the Ce–Ru–NCPs prepared under different experimental conditions (see Table 1 for details).

hybridized with S2-DA. After the magnetic separation and redispersion, 5 U·mL^{-1} Nt.BsmAl nick endonuclease was added and incubated at 37 °C for 1 h. During the cutting process, the two walker probes were released and entered the next walking process, and generated a large number of the secondary target DNA labeled with the quencher of DA (S3-DA). After the magnetic separation, the obtained S3-DA was stored at 4 °C for further use.

Assembly of the Biosensor. Before use, each bare glassy carbon electrode (GCE, Φ = 4.0 mm) was polished with 0.3 and 0.05 μm alumina slurry and washed with ethanol and water. The luminescent nanocomposite was obtained by

https://dx.doi.org/10.1021/acs.analchem.0c00130
Anal. Chem. 2020, 92, 12145−12151

mixing 100 μL of Ce−Ru−NCP (20 mg·mL^{-1}), 300 μL of nafion (NF, 1 wt%) and 300 μL of AuNPs into a centrifugation tube and shaken evenly. Subsequently, 5 μL of the above solution was dropped onto the surface of GCE and dried at room temperature (recorded as NF−AuNPs−Ce−Ru−NCP/GCE). Then, 10 μL of 2 μmol·L^{-1} thiol-modified DNA strand D1 was incubated on the NF−AuNPs−Ce−Ru−NCP/GCE at 4 °C overnight to obtain D1/NF−AuNPs−Ce−Ru−NCP/GCE via the Au−S bond. Also, 10 μL of 2 μmol·L^{-1} thiol-modified DNA strand D2 was used to block the nonspecific binding sites. Next, 10 μL of S3-DA was incubated on the surface of electrode for 2 h. S3-DA can hybridize with D1 to introduce massive DA onto the surface of the electrode, which can quench the ECL intensity of Ce−Ru−NCP, resulting in a significant decrease in the ECL signal.

RESULTS AND DISCUSSION

Schematic Diagram of the Manufacturing Process of the ECL Biosensor. As depicted in Scheme 1, the bipedal 3D DNA walking machine is prepared by connecting two separate 3D DNA walking machines (1 and 2) through two complementary DNA strands (A1 and A2). In the absence of miRNA-141, walker probes (walkers 1 and 2) are locked by the protect DNAs (protect 1 and 2) and the bipedal 3D DNA walking machine cannot work. In the presence of miRNA-141, walkers 1 and 2 are released, and, respectively, hybridized with support DNA 1 (S1-DA) and DNA 2 (S2-DA) to form two recognition sites. Then, they are sheared by Nt.BsmAl nick endonuclease, leading to the release of the two walker probes for the next walking process. The Nt.BsmAl nick endonuclease provides energy for walkers 1 and 2 to walk along their tracks autonomously and processively and achieves the massive release of secondary targets labeled by the quencher of dopamine (S3-DA). After S3-DA has been hybridized with D1, the ECL intensity of Ce−Ru−NCP is quenched, resulting in a significant decrease in the ECL response. The amplification strategy of the bipedal 3D DNA walking machine was verified by polyacrylamide gel electrophoresis (SI Figure S1). All DNA sequences are shown in SI Table S1.

Characterization of Ce−Ru−NCPs, AuNPs, and Au@PSC. The morphologies of the Ce−Ru−NCPs that are synthesized under different experimental conditions were characterized by scanning electron microscopy (SEM). The morphologies of Ce−Ru−NCPs are observed in various forms, including flower, honeycomb, hill, hump, flake, net, and snowlike (from Figure 1A−G). Using these Ce−Ru−NCPs as the ECL luminophores, the largest ECL intensity is obtained from the flowerlike Ce−Ru−NCP (Table 1). Considering the factors of solvent, yield, and ECL intensity, the flowerlike Ce−Ru−NCP was selected as the luminophore for further experiments. Meanwhile, AuNPs and Au@PSC were also characterized by SEM (SI Figure S2).

The synthesis of Ce−Ru−NCP was further confirmed by Fourier transform infrared (FTIR) (SI Figure S3A). Compared to those of Ru(dcbpy)$_3^{2+}$ (curve a), the O−H and C═O peaks (symmetric and antisymmetric stretching vibrations) of Ce−Ru−NCP (curve b) are shifted to 3396 and 1404 cm^{-1}, respectively. Besides, the new peak appearing at 453 cm^{-1} belonged to the O−Ce stretching vibration, indicating the coordination between −COOH and Ce^{3+}.

From the UV−vis absorption spectra (SI Figure S3B), the peaks of $Ce(NO_3)_3$ at 214 and 295 nm are attributed to the $\pi \rightarrow \pi^*$ electron transition of the nitrate ion and the 4f−5d transition of Ce^{3+}, respectively. Two peaks at 303 and 473 nm are observed for Ru(dcbpy)$_3^{2+}$ owing to the carboxyl and bipyridyl rings groups, respectively. However, after the formation of Ce−Ru−NCP, the peak at 214 nm for the nitrate ion disappeared as well as the other two peaks are blue-shifted to 300 and 471 nm. The above results show the coordination between Ru(dcbpy)$_3^{2+}$ and Ce^{3+}.

The Ce−Ru−NCP was also investigated by the energy-dispersive X-ray (EDX) spectroscope, X-ray photoelectron spectroscopy (XPS), X-ray diffraction (XRD), and selected-area electron diffraction (SAED). According to the literature, the center Ce^{3+} of Ce−Ru−NCP is nine coordinated, in which six oxygen atoms are from the water molecule and three oxygen atoms are from the carboxyl groups of the Ru(dcbpy)$_3^{2+}$ ligand[16] (Figure 2). From SI Figure S3C, the strong

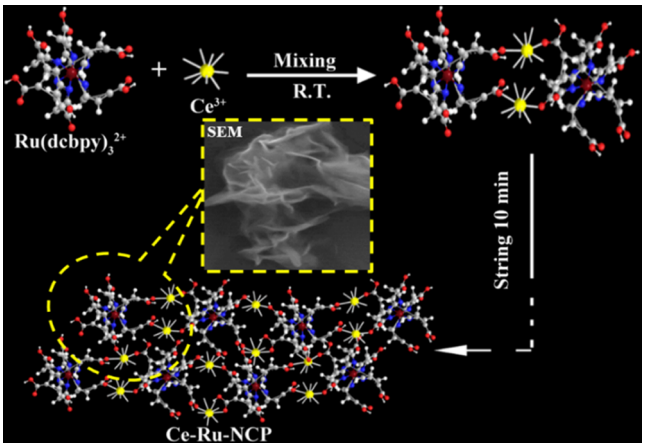

Figure 2. Schematic illustration of the preparation of Ce−Ru−NCP. Inset is the SEM of Ce−Ru−NCP.

and broad peak at about 21.1°, which corresponds to a crystalline interplanar spacing of 3.1 Å, indicates that Ce−Ru−NCP possesses an amorphous structure and that $\pi-\pi$ stacking plays a key role in the formation of the flowerlike Ce−Ru−NCP.[15,16] From SI Figure S3D, Ce−Ru−NCP is found to have a complicated structure, which is hard to analyze with the existing technology. The results from EDX and XPS (SI Figures S4 and S5) show that the material consists of C, N, O, Ru, and Ce elements. All of the above characterizations suggest the successful preparation of Ce−Ru−NCP.

The ECL emission spectrum of the Ce−Ru−NCP/$S_2O_8^{2-}$ system was measured by NF−AuNPs−Ce−Ru−NCP/GCE in 6.0 mmol·L^{-1} $K_2S_2O_8$ (20 mmol·L^{-1} Tris−HCl, pH 7.0). The 3D surface image model (Figure 3A), the heat map of the ECL potential wavelength image (Figure 3B), and the two-dimensional (2D) ECL spectrum (Figure 3C, curve b) show the maximum ECL emission wavelength (λ_{max}) at 729 nm. A significant red shift of about 136 nm appeared compared with the typical Ru(dcbpy)$_3^{2+}$/$S_2O_8^{2-}$ system (λ_{max} = 593 nm; Figure 3C, curve a, measured via GCE in 10 mmol·L^{-1} Ru(dcbpy)$_3^{2+}$ containing 6.0 mmol·L^{-1} $K_2S_2O_8$ (20 mmol·L^{-1} Tris−HCl, pH 7.0)). The intensity−wavelength curve is based on the following formula[17]

$$I = \frac{Nh}{\lambda A t} \quad (1)$$

where I, λ, h, A, t, and N are the intensity, wavelength, Planck constant, irradiation area, time, and the total number of

https://dx.doi.org/10.1021/acs.analchem.0c00130
Anal. Chem. 2020, 92, 12145−12151

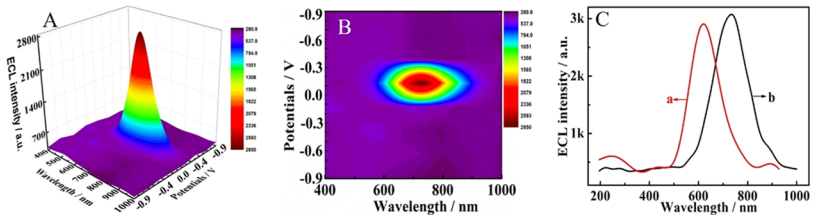

Figure 3. (A) 3D surface image model and (B) heat map image of the ECL potential wavelength of NF−AuNPs−Ce−Ru−NCP/GCE. (C) 2D ECL spectra of (a) GCE in 10 mmol·L^{-1} Ru(dcbpy)$_3^{2+}$ and (b) the NF−AuNPs−Ce−Ru−NCP/GCE.

photons reaching A in the time interval *t*. The $\sum_{\lambda=450}^{900} I/I_{total}$ values of Ce−Ru−NCP and Ru(dcbpy)$_3^{2+}$ are calculated to be 82.1 and 81.7%, respectively. These results show that the red shift in the ECL spectrum is contributed by the energy change of some photons and indicate that Ru(dcbpy)$_3^{2+}$ acts as an organic ligand in Ce−Ru−NCP.[17]

Characterization of Different Modified Electrodes. From the results of cyclic voltammetry (CV) and electrochemical impedance spectroscopy (EIS), the proposed biosensor was successfully prepared (SI Figure S6). The ECL intensity of different modified electrodes was also tested. As presented in Figure 4A, almost no ECL signal is observed on the bare GCE (curve a), while the ECL signal is significantly improved on the NF−AuNPs−Ce−Ru−NCP−modified GCE (curve b). According to eq 1 (SI eq 1), the ECL efficiency of the Ce−Ru−NCP/$S_2O_8^{2-}$ system was calculated. It is about 2.34 times that of the Ru(bpy)$_3^{2+}$/$S_2O_8^{2-}$ system, suggesting that the ECL efficiency can be improved by Ce−Ru−NCP remarkably. The reasons may be as follows: (1) The fluorescence (FL) emission spectrum of Ce^{3+} overlaps with the FL excitation spectrum of Ru(dcbpy)$_3^{2+}$ (SI Figure S7), displaying the presence of energy transfer between Ce^{3+} and Ru(dcbpy)$_3^{2+}$. That is to say, Ce^{3+} acts as a sensitizer for the luminescent of Ru(dcbpy)$_3^{2+}$.[29−31] (2) Ce^{3+}, as a co-reaction accelerator, can react with $S_2O_8^{2-}$ to produce more sulfate radical anions ($SO_4^{\bullet-}$) and accelerate the electrochemical reaction rate of Ce−Ru−NCP and $S_2O_8^{2-}$, which can amplify the ECL efficiency.[32,33] (3) The potential sweep range of Ce−Ru−NCP (0 to −0.9 V) is narrower than that of traditional cathodic luminophores, such as quantum dots, metal nanoclusters, tetraphenylethene derivatives, Ru(bpy)$_3^{2+}$, and so on.[3−6] This avoids the damage of the modified electrodes and biomolecules and improves the stability and repeatability of the biosensor.[1,3] Furthermore, the electrochemistry and the ECL behavior of Ce−Ru−NCP in the absence and presence of 6.0 mmol·L^{-1} $S_2O_8^{2-}$ were also investigated (SI Figure S8).

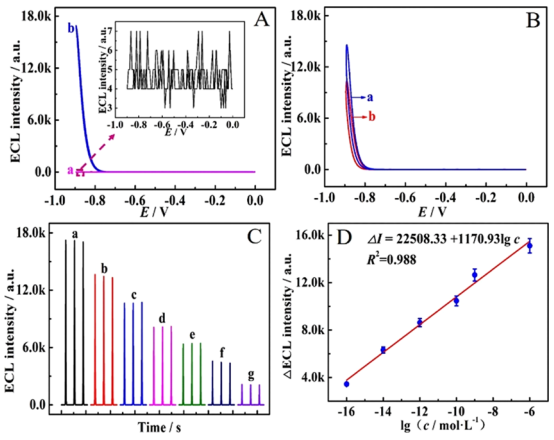

Figure 4. (A) ECL responses to (a) bare GCE and (b) NF−AuNPs−Ce−Ru−NCP/GCE. (B) ECL responses of the biosensor with the aid of 3D DNA walking machine: (a) the single foot and (b) the bipedal (in 1.0 × 10^{-13} mol·L^{-1} miRNA-141). (C) ECL responses of the proposed biosensor in different concentrations of miRNA-141: (a) 0, (b) 1.0 × 10^{-16}, (c) 1.0 × 10^{-14}, (d) 1.0 × 10^{-12}, (e) 1.0 × 10^{-10}, (f) 1.0 × 10^{-9}, and (g) 1.0 × 10^{-6} mol·L^{-1}. (D) Plots of Δ*I* vs the logarithm of miRNA-141 concentration.

The control experiments were carried out to reveal the amplification effect of the 3D DNA walking machine. As presented in Figure 4B, with the aid of the single-foot (curve a) or the bipedal 3D DNA walking machine (curve b), the ECL intensities of the biosensor are quenched to 15494 and 11137 au, respectively, hinting that the bipedal 3D DNA walking machine possesses a higher shearing efficiency and can produce more DA quencher labeled secondary targets.

Analytical Performance of the ECL Biosensor. Under optimal experimental conditions (SI Figures S9 and S10), with the increasing concentration of miRNA−141 from 1.0 × 10^{-16} to 1.0 × 10^{-6} mol·L^{-1}, the ECL intensity gradually decreases (Figure 4C,D). The ECL intensity difference ($\Delta I = I_0 - I$, where I_0 and I are the ECL intensities of the proposed biosensors incubated with blank and different miRNA-141 concentrations, respectively) shows a good linear relationship to the logarithmic value of the miRNA-141 concentration. The

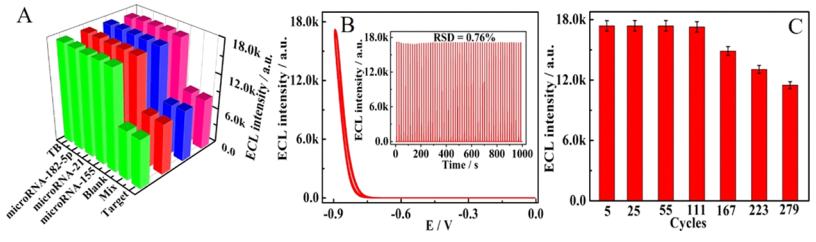

Figure 5. (A) Selectivity of the proposed biosensor: blank sample, 1.0 × 10^{-9} mol·L^{-1} interfering substances, including TB, microRNA-182−5P, microRNA-21, and microRNA-155, 1.0 × 10^{-12} mol·L^{-1} target miRNA-141, and the mixture (1.0 × 10^{-12} mol·L^{-1} target miRNA-141 and 1.0 × 10^{-9} mol·L^{-1} interfering substances). Stability of the proposed biosensor under consecutive cyclic potential scans for (B) 56 and (C) 279 cycles.

https://dx.doi.org/10.1021/acs.analchem.0c00130
Anal. Chem. 2020, 92, 12145−12151

regression equation is determined as follows: $\Delta I = 22\,508.33 + 1170.93 \lg c$ ($R^2 = 0.988$) with the limit of detection (LOD) of 33 amol·L^{-1} ($S/N = 3$). From the SI Table S2 and S3, the proposed biosensor shows an enhanced sensitivity compared with other methods.

Selectivity, Stability, and Reproducibility of the ECL Biosensor. Selectivity is one of the main parameters for evaluating the anti-interference ability of the ECL biosensor. Therefore, some high concentrations possible of interfering substances including microRNA-155, microRNA-21, microRNA-182−5P, and specific protein thrombin (TB) were selected. As evidenced by Figure 5A, the ECL signals similar to those of the blank appear with the addition of the relatively high concentrations of interfering substances (1.0×10^{-9} mol·L^{-1}), whereas a significantly decreased ECL signal obtained when the target miRNA-141 is presented even at a lower concentration (1.0×10^{-12} mol·L^{-1}) or the mixture (1.0×10^{-12} mol·L^{-1} miRNA-141 mixed with 1.0×10^{-9} mol·L^{-1} interfering substances). These results, as expected, clearly demonstrate a good selectivity of this proposed biosensor for miRNA-141 determination. Similarly, stability is another important parameter of the ECL biosensor, which was evaluated by periodically scanning 56 cycles for 1000 s (Figure 5B). The relative standard deviation (RSD) is 0.76%. Besides, the ECL intensities only decreased by 14.1% after 167 cycles and 33.7% after 279 cycles (Figure 5C). The RSD of seven batches of modified electrodes prepared at different times is 0.8%. Meanwhile, the assay in diluted human serum (SI Table S4) and nuclear extraction of the cancer cells (SI Figure S11) were conducted to demonstrate that this proposed sensing system can detect miRNA-141 in biological samples.

CONCLUSIONS

In summary, based on this novel luminophore of Ce−Ru−NCP and the amplification technique of the bipedal 3D DNA walking machine, an ECL biosensor is constructed and applied to detect miRNA-141. The biosensor possesses three novel ideas: (1) the synthesis method of Ce−Ru−NCP is simple, rapid, mild, high yielding, reproducible, room temperature, and environmentally friendly. (2) Ce−Ru−NCP has a higher ECL efficiency, a more stable ECL signal, and a lower potential than the traditional cathodic ECL luminophores. (3) The amplification technique of the bipedal 3D DNA walking machine further improves the sensitivity of the ECL biosensor. Overall, this work provides a new Ce−Ru−NCP luminophore and extends the application of the 3D DNA walking machine in the ECL biosensor, which may offer a sensitive and efficient method in electrical analysis and biological analysis.

ASSOCIATED CONTENT

Supporting Information

The Supporting Information is available free of charge at https://pubs.acs.org/doi/10.1021/acs.analchem.0c00130.

Reagents and apparatus, ECL measurement procedure, synthesis of AuNPs and Au@PSC, polyacrylamide gel electrophoresis (PAGE) characterization, characterization of Ce−Ru−NCP, AuNPs, and Au@PSC, fluorescence spectrum, ECL efficiency of the Ce−Ru−NCP/$S_2O_8^{2-}$ system, electrochemical performance of the stepwise modified electrodes, optimization of the experimental conditions, and application of the proposed biosensor (PDF)

AUTHOR INFORMATION

Corresponding Author

Yingzi Fu − *Chongqing Engineering Laboratory of Nanomaterials & Sensor Technologies, School of Chemistry and Chemical Engineering, Southwest University, Chongqing 400715, China;* orcid.org/0000-0003-4894-8549; Phone: +86-023-68252277; Email: fyzc@swu.edu.cn

Authors

Cun Wang − *Chongqing Engineering Laboratory of Nanomaterials & Sensor Technologies, School of Chemistry and Chemical Engineering, Southwest University, Chongqing 400715, China; Chongqing Collaborative Innovation Center for Functional Food, Chongqing University of Education, Chongqing 400067, China*

Qian Han − *Chongqing Engineering Laboratory of Nanomaterials & Sensor Technologies, School of Chemistry and Chemical Engineering, Southwest University, Chongqing 400715, China; Laboratory of Environment Change and Ecological Construction of Hebei Province, College of Resources and Environment Science, Hebei Normal University, Shijiazhuang, Hebei 050024, China*

Fangjing Mo − *Chongqing Engineering Laboratory of Nanomaterials & Sensor Technologies, School of Chemistry and Chemical Engineering, Southwest University, Chongqing 400715, China*

Min Chen − *Chongqing Engineering Laboratory of Nanomaterials & Sensor Technologies, School of Chemistry and Chemical Engineering, Southwest University, Chongqing 400715, China*

Zhengwei Xiong − *Chongqing Collaborative Innovation Center for Functional Food, Chongqing University of Education, Chongqing 400067, China*

Complete contact information is available at: https://pubs.acs.org/10.1021/acs.analchem.0c00130

Notes

The authors declare no competing financial interest.

ACKNOWLEDGMENTS

This work is supported by the National Natural Science Foundation of China (21272188) and the Science and Technology Research Project of the Chongqing Municipal Education Commission (KJQN201901604).

REFERENCES

(1) Song, Y.; Zhang, W.; He, S. J.; Shang, L.; Ma, R. N.; Jia, L. P.; Wang, H. S. *ACS Appl. Mater. Interfaces* **2019**, *11*, 33676−33683.

(2) Ma, C.; Cao, Y.; Gou, X. D.; Zhu, J. J. *Anal. Chem.* **2020**, *92*, 431−454.

(3) Chen, A. Y.; Liang, W. B.; Wang, H. J.; Zhuo, Y.; Chai, Y. Q.; Yuan, R. *Anal. Chem.* **2020**, *92*, 1379−1385.

(4) Zhao, Y. R.; Yu, J.; Xu, G. B.; Sojic, N.; Loget, G. *J. Am. Chem. Soc.* **2019**, *141*, 13013−13016.

(5) Yan, M. X.; Ye, J.; Zhu, Q. J.; Zhu, L. P.; Huang, J. S.; Yang, X. R. *Anal. Chem.* **2019**, *91*, 10156−10163.

(6) Wang, X.; Shang, L.; Zhang, W.; Jia, L. P.; Ma, R. N.; Jia, W. L.; Wang, H. S. *Biosens. Bioelectron.* **2019**, *141*, 111436−1114312.

(7) Hu, G. B.; Xiong, C. Y.; Liang, W. B.; Yang, Y.; Yao, L. Y.; H, W.; Luo, W.; Yuan, R.; Xiao, D. R. *Biosens. Bioelectron.* **2019**, *135*, 95−101.

(8) Dong, X.; Zhao, G. H.; Liu, L.; Li, X.; Wei, Q.; Cao, W. *Biosens. Bioelectron.* **2018**, *110*, 201−206.

(9) Chen, A.; Zhao, M.; Zhuo, Y.; Chai, Y. Q.; Yuan, R. *Anal. Chem.* **2017**, *89*, 9232−9238.

(10) Shan, Y.; Wu, H. Y.; Xiong, S. J.; Wu, X. L.; Chu, P. K. *Angew. Chem. Int. Ed.* **2016**, *55*, 2017−2021.
(11) Song, F.; Wang, C.; Falkowski, J. M.; Ma, L.; Lin, W. *J. Am. Chem. Soc.* **2010**, *132*, 15390−15398.
(12) Zhu, S.; Lin, X.; Ran, P. Y.; Xia, Q.; Yang, C. C.; Ma, J.; Fu, Y. Z. *Biosens. Bioelectron.* **2017**, *91*, 436−440.
(13) Mancino, G.; Ferguson, A. J.; Beeby, A.; Long, N. J.; Jones, T. S. J. *J. Am. Chem. Soc.* **2005**, *127*, 524−525.
(14) Heffern, M. C.; Matosziuk, L. M.; Meade, T. J. *Chem. Rev.* **2014**, *114*, 4496−4539.
(15) Chen, W.; Yuan, H.-M.; Wang, J.-Y.; Liu, Z.-Y.; Yang, M. Y.; Chen, J.-S.; Xu, J.-J. *J. Am. Chem. Soc.* **2003**, *125*, 9266−9267.
(16) Liu, K.; You, H. P.; Jia, G.; Zheng, Y. H.; Huang, Y. J.; Song, Y. H.; Yang, M.; Zhang, L. H.; Zhang, H. J. *Cryst. Growth Des.* **2010**, *10*, 790−797.
(17) Xiong, C. Y.; Wang, H. J.; Liang, W. B.; Yuan, Y. L.; Yuan, R.; Chai, Y. Q. *Chem. − Eur. J.* **2015**, *21*, 9825−9832.
(18) Tang, J.; He, X.; Lei, Y.; Shi, H.; Guo, Q. P.; Liu, J. B.; He, D. G.; Yan, L.; Wang, K. *Chem. Commun.* **2017**, *53*, 11889−11892.
(19) Chang, C. C.; Chen, C. P.; Chen, C. Y.; Lin, C. W. *Chem. Commun.* **2016**, *52*, 4167−4170.
(20) Dai, W.; Dong, H.; Guo, K.; Zhang, X. *Chem. Sci.* **2018**, *9*, 1753−1759.
(21) Liao, H. X.; Zhou, Y.; Chai, Y. Q.; Yuan, R. *Biosens. Bioelectron.* **2018**, *114*, 10−14.
(22) Qing, M.; Xie, S. B.; Cai, W.; Tang, D. Y.; Tang, Y.; Zhang, J.; Yuan, R. *Anal. Chem.* **2018**, *90*, 11439−11445.
(23) Wu, T. T.; Cao, Y.; Yang, Y. M.; Zhang, X. Y.; Wang, S. T.; Xu, L. P.; Zhang, X. J. *Nanoscale.* **2019**, *11*, 11279−11284.
(24) Zhao, M.; Bai, L. J.; Cheng, W.; Duan, X. L.; Wu, H. P.; Ding, S. J. *Biosens. Bioelectron.* **2019**, *127*, 126−134.
(25) Feng, C.; Wang, Z. H.; Chen, T. S.; Chen, X. X.; Mao, D. S.; Zhao, J.; Li, G. X. *Anal. Chem.* **2018**, *90*, 2810−2815.
(26) Xu, X. W.; Zhang, P. P.; Zhang, R. Y.; Zhang, N.; Jiang, W. *Chem. Commun.* **2019**, *55*, 6026−6029.
(27) Yang, J. M.; Wu, Y. L.; Gan, C. F.; Yuan, R.; Xiang, Y. *Biosens. Bioelectron.* **2018**, *117*, 743−747.
(28) Ojea-Jiménez, I.; Romero, F. M.; Bastu′s, N. G.; Puntes, V. *J. Phys. Chem. C* **2010**, *114*, 1800−1804.
(29) Lai, H.; Bao, A.; Yang, Y. M.; Tao, Y. C.; Yang, H.; Zhang, Y.; Han, L. L. *J. Phys. Chem. C* **2008**, *112*, 282−286.
(30) Li, Q.; Yam, V. W. W. *Angew. Chem., Int. Ed.* **2007**, *46*, 3486−3489.
(31) Shionoya, S.; Nakazawa, E. *Appl. Phys. Lett.* **1965**, *6*, 118−128.
(32) Lei, Y. M.; Wen, R. X.; Zhou, J.; Chai, Y. Q.; Yuan, R.; Zhuo, Y. *Anal. Chem.* **2018**, *90*, 6851−6858.
(33) Dong, C. D.; Chen, C. W.; Nguyen, T. B.; Huang, C. P.; Hung, C. M. *Chem. Eng. J.* **2020**, *384*, No. 123301.

https://dx.doi.org/10.1021/acs.analchem.0c00130
Anal. Chem. 2020, 92, 12145−12151